

Supporting Information of

Creating Glassy States of Dicarboxylate-bridged Coordination Polymers

Zeyu Fan,^a Yong-Sheng Wei,^b Chinmoy Das,^b Kazuyoshi Kanamori,^c Hiroki Yamada,^d Koji Ohara^d and Satoshi Horike^{*bce}

^a *Department of Synthetic Chemistry and Biological Chemistry, Graduate School of Engineering, Kyoto University, Katsura, Nishikyo-ku, Kyoto 615-8510, Japan*

^b *Institute for Integrated Cell-Material Sciences, Institute for Advanced Study, Kyoto University, Yoshida-Honmachi, Sakyo-ku, Kyoto 606-8501, Japan.*

^c *Department of Chemistry, Graduate School of Science, Kyoto University, Kitashirakawa-Oiwakecho, Sakyo-ku, Kyoto 606-8502, Japan.*

^d *Diffraction and Scattering Division, Japan Synchrotron Radiation Research Institute (JASRI), Sayo, Hyogo 679-5198, Japan.*

^e *Department of Materials Science and Engineering, School of Molecular Science and Engineering, Vidyasirimedhi Institute of Science and Technology, Rayong, 21210, Thailand*

*Email: horike.satoshi.3r@kyoto-u.ac.jp (S.H)

Table of contents

Experimental section	S2-S4
Supplementary figures	S6-S25
Supplementary tables	S26-S27
References	S28

Experimental

1. Materials and experimental methods

All reagents and chemicals were obtained from commercial sources and used without further purification. $\text{Mn}(\text{NO}_3)_2 \cdot 6\text{H}_2\text{O}$ (98%), $\text{Co}(\text{NO}_3)_2 \cdot 6\text{H}_2\text{O}$ (98%), $\text{Ni}(\text{NO}_3)_2 \cdot 6\text{H}_2\text{O}$ (97%), $\text{Cd}(\text{NO}_3)_2 \cdot 4\text{H}_2\text{O}$ (99%), 4,4'-Bipyridyl (bpy, 97%), disodium terephthalate (Na_2bdc , 99%), disodium fumarate (Na_2fum , 98%), tetrahydrofuran (THF, 99%) and diethyl ether (Et_2O , 99.5%) were purchased from Wako. Trans-1,2-bis(4-pyridyl)ethylene (bpee, 98%) was purchased from TCI.

a) Synthesis of $[\text{Co}(\text{bpy})(\text{H}_2\text{O})_4] \cdot \text{fum} \cdot 4\text{H}_2\text{O} (1 \cdot \text{H}_2\text{O})$

$\text{Co}(\text{NO}_3)_2 \cdot 6\text{H}_2\text{O}$ (1 mmol), Na_2fum (1 mmol) and bpy (1 mmol) were added in DI water (20 mL) and stirred at room temperature overnight. The product was washed with DI water, THF and Et_2O and stored in open air to give $1 \cdot \text{H}_2\text{O}$ (453 mg, 96% yield based on metal).

b) Synthesis of $[\text{Co}(\text{bpy})(\text{H}_2\text{O})_4] \cdot \text{bdc} (2 \text{ H}_2\text{O})$

$\text{Co}(\text{NO}_3)_2 \cdot 6\text{H}_2\text{O}$ (1 mmol), Na_2bdc (1 mmol) and bpy (1 mmol) were added in DI water (20 mL) and stirred at room temperature overnight. The product was washed with DI water, THF and Et_2O and stored in open air to give $2 \text{ H}_2\text{O}$ (425 mg, 94% yield based on metal). Use $\text{Mn}(\text{NO}_3)_2 \cdot 6\text{H}_2\text{O}$, $\text{Ni}(\text{NO}_3)_2 \cdot 6\text{H}_2\text{O}$, and $\text{Cd}(\text{NO}_3)_2 \cdot 4\text{H}_2\text{O}$ as metal salt provided $2 \text{ H}_2\text{O}(\text{Mn})^1$, $2 \text{ H}_2\text{O}(\text{Ni})$ and $2 \text{ H}_2\text{O}(\text{Cd})^2$.

c) Synthesis of $[\text{Co}(\text{bpee})(\text{H}_2\text{O})_4] \cdot \text{bdc} \cdot 2\text{H}_2\text{O} (3 \text{ H}_2\text{O})$

$\text{Co}(\text{NO}_3)_2 \cdot 6\text{H}_2\text{O}$ (1 mmol), Na_2bdc (1 mmol) and bpee (1 mmol) were added in DI water (20 mL) and stirred at room temperature overnight. The product was washed with DI water, THF and Et_2O and stored in open air to give $3 \text{ H}_2\text{O}$ (412 mg, 80% yield based on metal).

d) Glass formation

Crystalline $1 \cdot \text{H}_2\text{O}$, $2 \cdot \text{H}_2\text{O}$, $2 \cdot \text{H}_2\text{O}(\text{M})$ ($\text{M} = \text{Mn}^{2+}$, Ni^{2+} , Cd^{2+}) and $3 \cdot \text{H}_2\text{O}$ were dried at 150 °C in vacuum overnight to give the glassy states $1\text{g}(\text{Co})$, $2\text{g}(\text{Co})$, $2\text{g}(\text{M})$ ($\text{M} = \text{Mn}^{2+}$, Ni^{2+} , Cd^{2+}) and $3\text{g}(\text{Co})$.

e) Preparation of glass monolith

Glass powder was deposited between two 10 mm highly polished stainless-steel disks and inserted in pellet DIE, which usually used for KBr pellet production for FTIR analysis

samples. The pellet DIE was then transferred to hot press machine and preheated at 160 °C for 30 min in vacuum and then pressure with 45 kN was added. Glass monolith was obtained after pressing 120 min at 160 °C.

2. Physical measurements

a) Powder X-ray diffraction (PXRD) patterns were recorded on a Rigaku MiniFlex 600 operated at 40 kV and 15 mA with Cu $K\alpha$ radiation ($\lambda = 1.54 \text{ \AA}$).

b) Thermogravimetric analysis (TGA) in air was carried out using a Rigaku Thermoplus 8120 under nitrogen atmospheres. TGA in Ar was carried out using a Rigaku Thermoplus 8120 that placed in glove box filled with Ar. A weighed sample in an aluminum pan was heated from 30 to 500 °C with heating rate of 10 °C min⁻¹. The weight loss of water in **1·H₂O**, **2·H₂O**, and **3·H₂O** were calculated based on their chemical formulas, the details are as follows:

$$\text{For } \mathbf{1 \cdot H_2O}, \text{ weight loss (H}_2\text{O)} = \frac{m_w(\text{H}_2\text{O}) \times 8}{m_w(\mathbf{1 \cdot H_2O})} = \frac{18 \times 8}{473.3} \times 100\% = 30.4\%$$

$$\text{For } \mathbf{2 \cdot H_2O}, \text{ weight loss (H}_2\text{O)} = \frac{m_w(\text{H}_2\text{O}) \times 4}{m_w(\mathbf{2 \cdot H_2O})} = \frac{18 \times 4}{451.2} \times 100\% = 15.9\%$$

$$\text{For } \mathbf{3 \cdot H_2O}, \text{ weight loss (H}_2\text{O)} = \frac{m_w(\text{H}_2\text{O}) \times 6}{m_w(\mathbf{3 \cdot H_2O})} = \frac{18 \times 6}{513.3} \times 100\% = 21.0\%$$

c) Differential scanning calorimetry (DSC) was measured with Hitachi High-Tech Science Corporation DSC7020. A weighed sample was measured with Ar flow.

d) Scanning electronic microscopy (SEM) observation was carried out by JEOL Model JSM-7001F4 SEM system operating at 15.0 kV. The samples were deposited on carbon tape and coated with osmium prior to the measurement.

e) Fourier-transform infrared spectroscopy (FT-IR) measurements were carried out using JASCO FTIR-6700 under Ar between the wavelength of 400 and 4000 cm⁻¹.

f) Gas adsorption isotherms were measured by BEL-max (Microtrac BEL Corp., Japan) gas adsorption instruments. The micropore volume (V_{pore}) was determined by the following equation³:

$$V_{\text{pore}} = \frac{n_{\text{ads}}^{\text{max}} \times M_{\text{CO}_2}}{\rho_{\text{sl}}} \quad (1)$$

in which the $n_{\text{ads}}^{\text{max}}$ is the specific CO₂ uptake amount (mmol g⁻¹) at 195 K and 95 kPa, M_{CO_2} is the molar mass of CO₂, ρ_{sl} is the density of the supercooled liquid at 195 K (1.258 g cm⁻³).

g) X-ray Absorption Fine-Structure (XAFS) was collected at 25 °C on beamline BL01B1 at SPring-8 (Hyogo, Japan). X-ray absorption spectra in the energy region of the Co K-edge were measured in transmission mode. Fourier transformation was k^3 -weighted in the k range from 3.0 to 10.5 \AA^{-1} . The data processing and coordination number fitting were performed with Athena and Artemis software, respectively. All samples were measured in Ar at 25 °C. The resulting k^3 -weighted radial distribution function was fitted by a FEFF calculation using single crystal data.

h) X-ray total scattering data was collected at 25 °C with four CdTe and two Ge detectors covering the Q range up to 25 \AA^{-1} at the BL04B2 beamline (61.377 keV) at SPring-8. Samples were packed in a quartz glass capillary ($\phi = 2$ mm) filled with argon. The incident beam was monochromated at $\lambda = 0.2020$ \AA . The collected scattering data was processed by the absorption, background, and Compton scattering corrections, and was then normalized to obtain the Faber-Ziman total structure factor ($S(Q)$).⁴ $G(r)$ is obtained from the Fourier transformation of $S(Q)$ with q range from 0.2 to 23 \AA with a Lorch modification function⁵ through Igor Pro software.⁶

i) Indentation measurements of the glass monoliths were performed by Shimazu DUH-211S, equipped with a three-sided Berkovich diamond tip. The glass monoliths were polished prior to the measurements. Values of H were determined by the following equation:

$$H = \alpha \frac{F}{h^2} \quad (2)$$

where the F is load, h is displacement into glass surface, α is constant dependent on the type of tip.

Young's modulus was calculated from the reduced modulus E_r , which reflects the combined elastic response of the Berkovich diamond indenter ($r = 0.1$ μm , $E_i = 1140$ GPa, $\nu_i = 0.07$) and the material tested:

$$E = (1 - \nu^2) \left[\frac{1}{E_r} - \frac{1 - \nu_i^2}{E_i} \right]^{-1} \quad (3)$$

Poisson ratio $\nu = 0.35$ was used.

Supplementary Figures

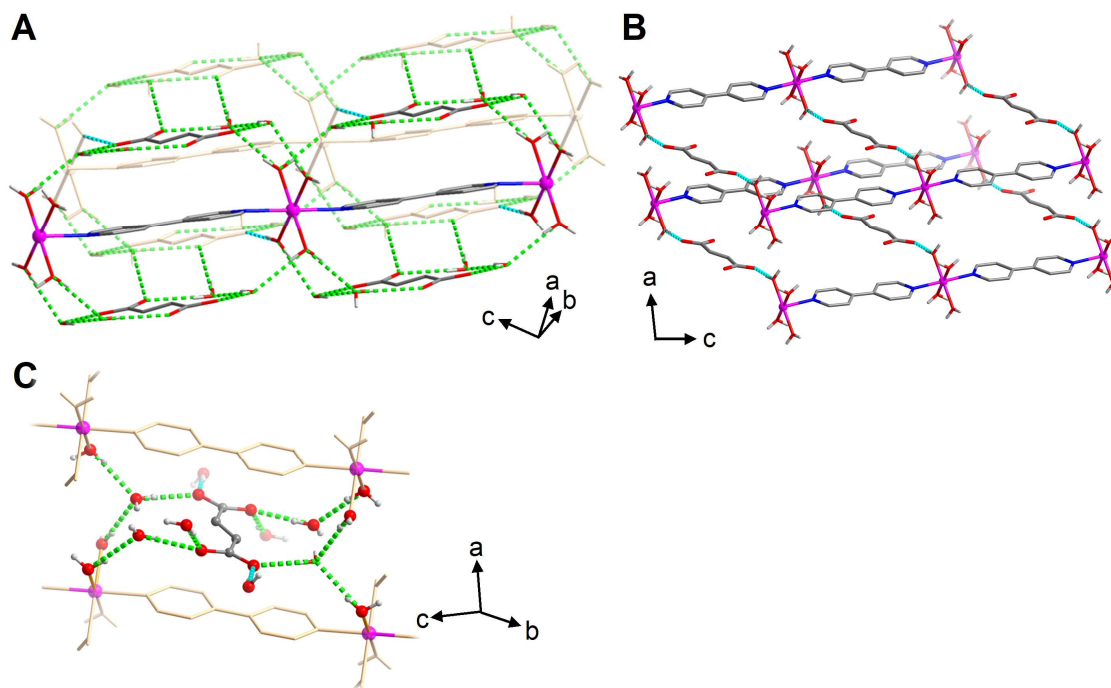


Fig. S1. (A) Crystal structure of $[\text{Co}(\text{bpy})(\text{H}_2\text{O})_4]\cdot\text{fum}\cdot 4\text{H}_2\text{O}$ ($1\cdot\text{H}_2\text{O}$). (B) Hydrogen bonds interactions between 1D $[\text{Co}(\text{bpy})(\text{H}_2\text{O})_4]^{2+}$ chains and fum. (C) Hydrogen bond interactions between fum and surrounded H_2O molecules. Hydrogen bond interactions between fum and coordinated H_2O are shown as blue dotted lines. Other hydrogen bond interactions are shown as green dotted lines. C, H, O, N and Co atoms are gray, white, red, blue and violet, respectively. H atoms on bpy and fum ligands are omitted for clarity.

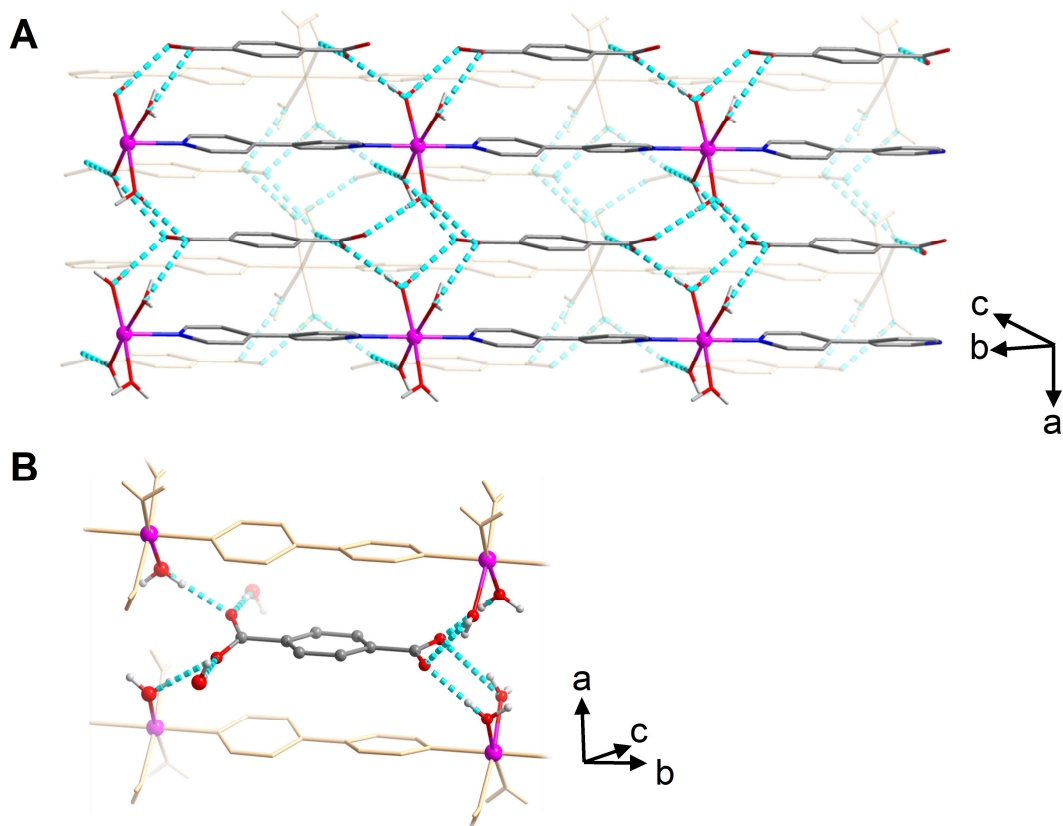


Fig. S2. (A) Crystal structure of [Co(bpy)(H₂O)₄]·bdc (2·H₂O). (B) Hydrogen bond interactions between bdc and surrounded H₂O molecules. Hydrogen bond interactions between bdc and coordinated H₂O are shown as blue dotted lines. C, H, O, N and Co atoms are gray, white, red, blue and violet, respectively. H atoms on bpy and bdc ligands are omitted for clarity.

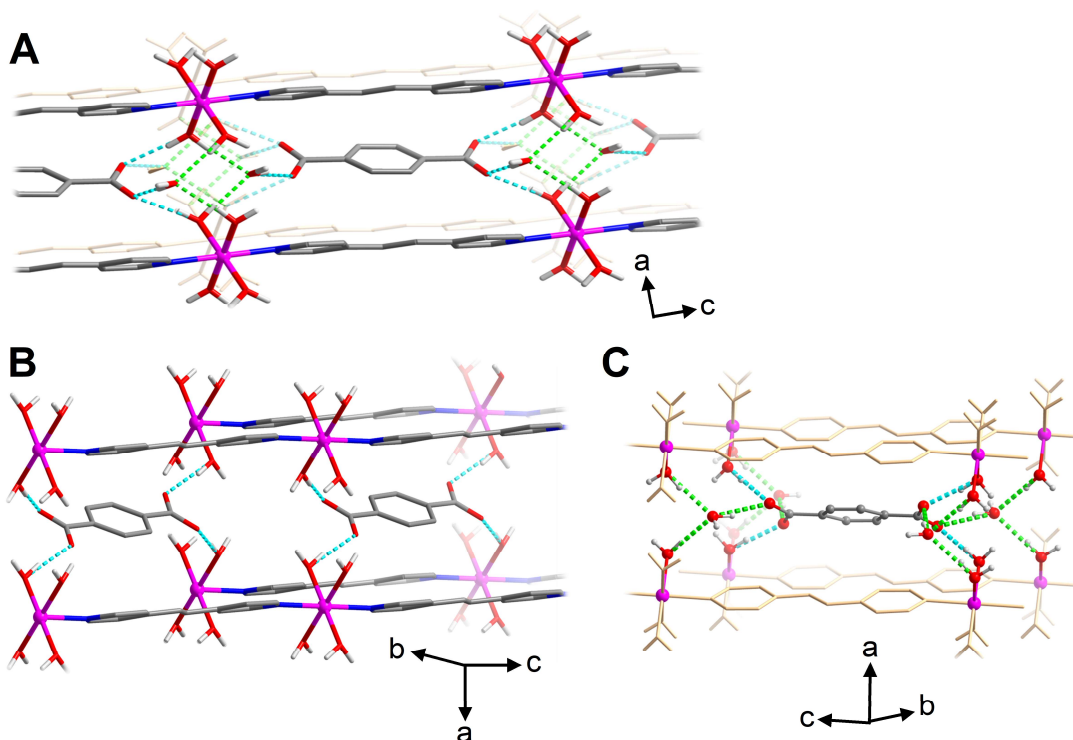


Fig. S3. (A) Crystal structure of $[\text{Co}(\text{bpee})(\text{H}_2\text{O})_4]\cdot\text{bdc}\cdot 2\text{H}_2\text{O}$ (**3** $\cdot\text{H}_2\text{O}$). (B) Hydrogen bonds interactions between 1D $[\text{Co}(\text{bpee})(\text{H}_2\text{O})_4]^{2+}$ chains and bdc. (C) Hydrogen bond interactions between bdc and surrounded H_2O molecules. Hydrogen bonds between bdc and H_2O are shown as sky blue dotted lines. Hydrogen bond interactions between H_2O molecules are shown as green dotted lines. C, H, O, N and Co atoms are gray, white, red, blue and violet, respectively. H atoms on bpee and bdc ligands are omitted for clarity.

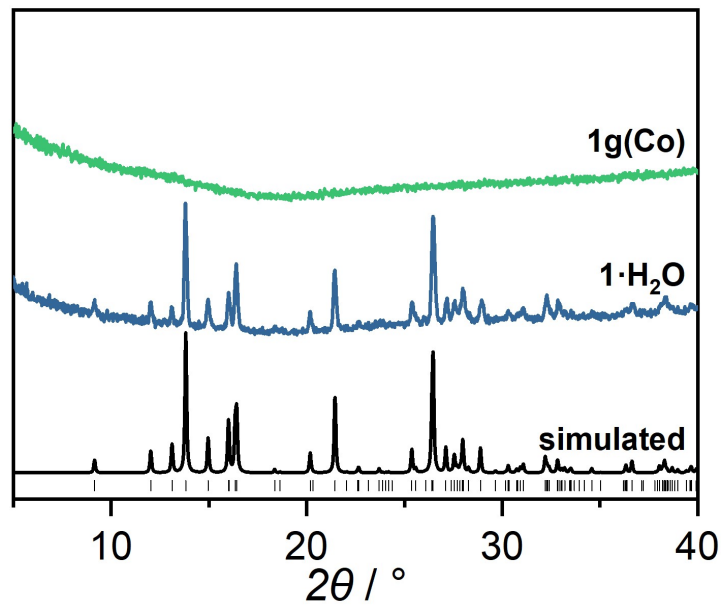


Fig. S4. PXRD patterns of simulated and as-synthesized **1·H₂O** and **1g(Co)**.

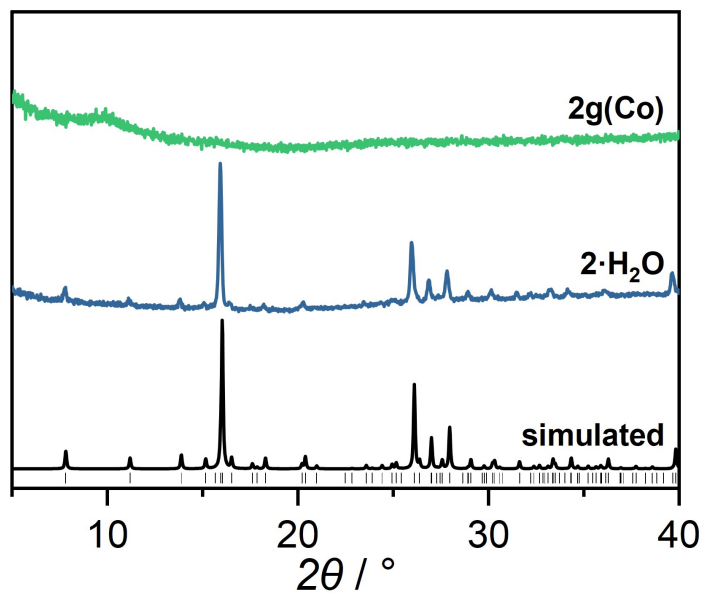


Fig. S5. PXRD patterns of simulated and as-synthesized **2·H₂O** and **2g(Co)**.

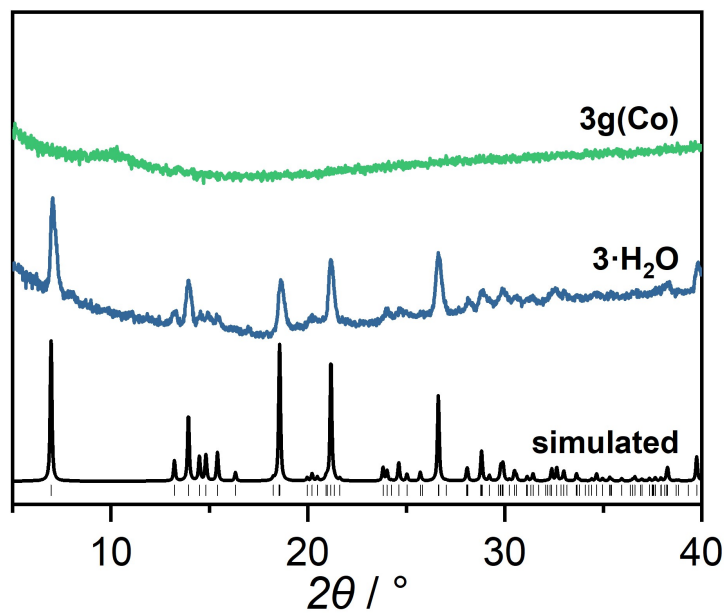


Fig. S6. PXRD patterns of simulated and as-synthesized $3\cdot\text{H}_2\text{O}$ and $3g(\text{Co})$.

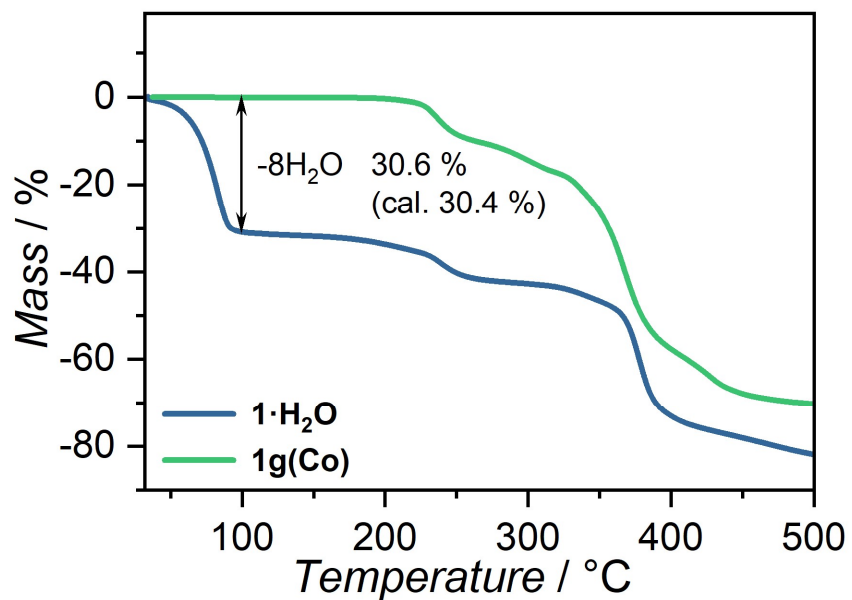


Fig. S7. TGA profiles of $1\cdot\text{H}_2\text{O}$ and $1g(\text{Co})$ measured with Ar flow. Heating rates were $10^\circ\text{C min}^{-1}$.

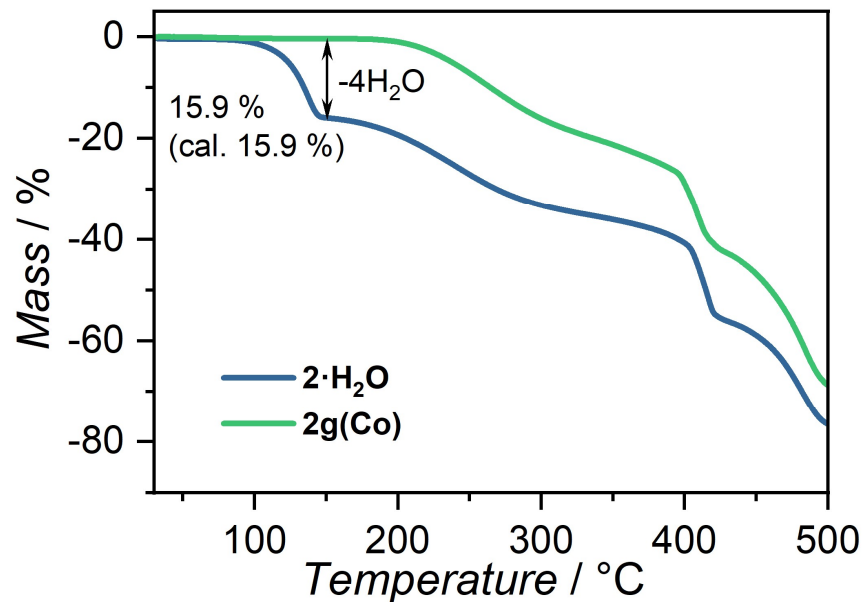


Fig. S8. TGA profiles of $2 \cdot \text{H}_2\text{O}$ and $2\text{g}(\text{Co})$ measured with Ar flow. Heating rates were $10 \text{ }^\circ\text{C min}^{-1}$.

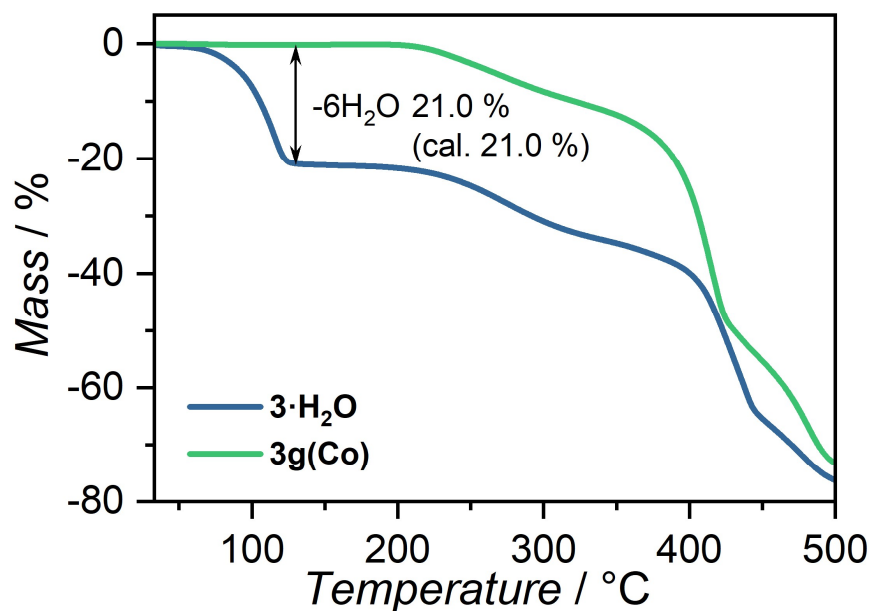


Fig. S9. TGA profiles of $3 \cdot \text{H}_2\text{O}$ and $3\text{g}(\text{Co})$ measured with Ar flow. Heating rates were $10 \text{ }^\circ\text{C min}^{-1}$.

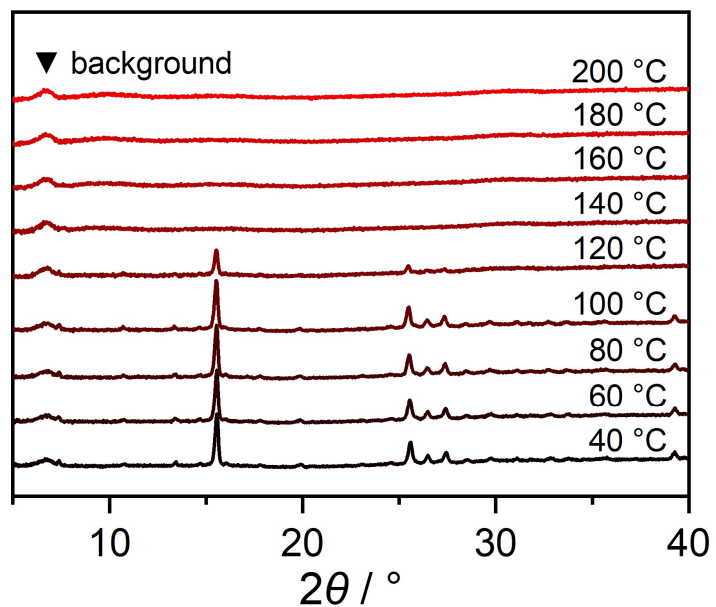


Fig. S10. VT-PXRD patterns of $2 \cdot \text{H}_2\text{O}$ from 40 to 180 °C measured with Ar flow.

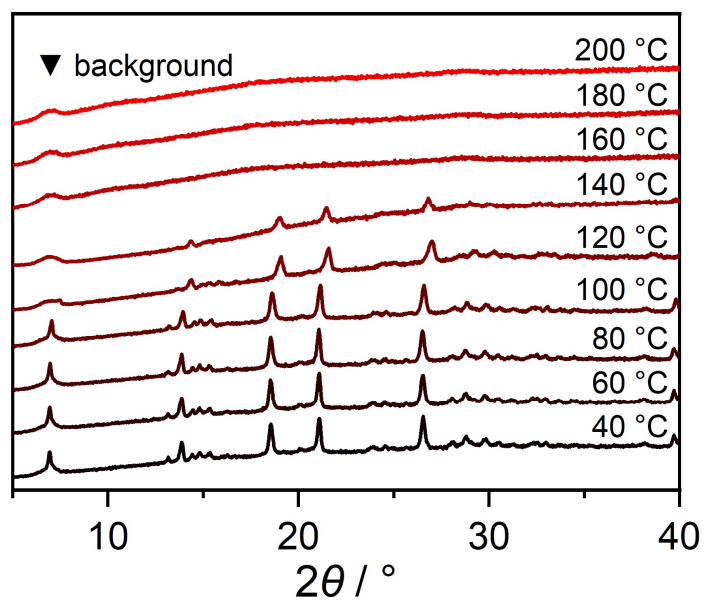


Fig. S11. VT-PXRD patterns of $3 \cdot \text{H}_2\text{O}$ from 40 to 180 °C measured with Ar flow.

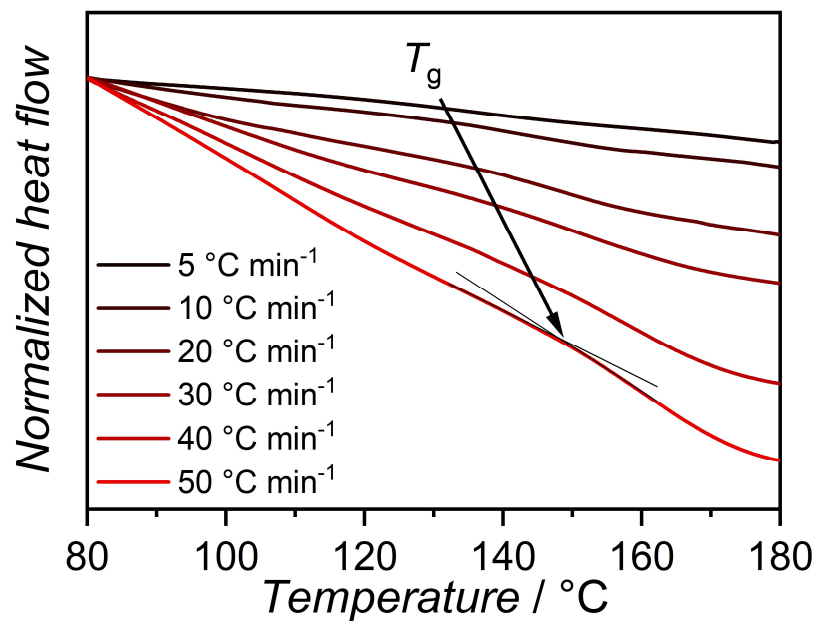


Fig. S12. DSC profiles from 80 to 180 °C of **1g(Co)** with Ar flow. Heating rates were in the range of 5 to 50 °C min⁻¹.

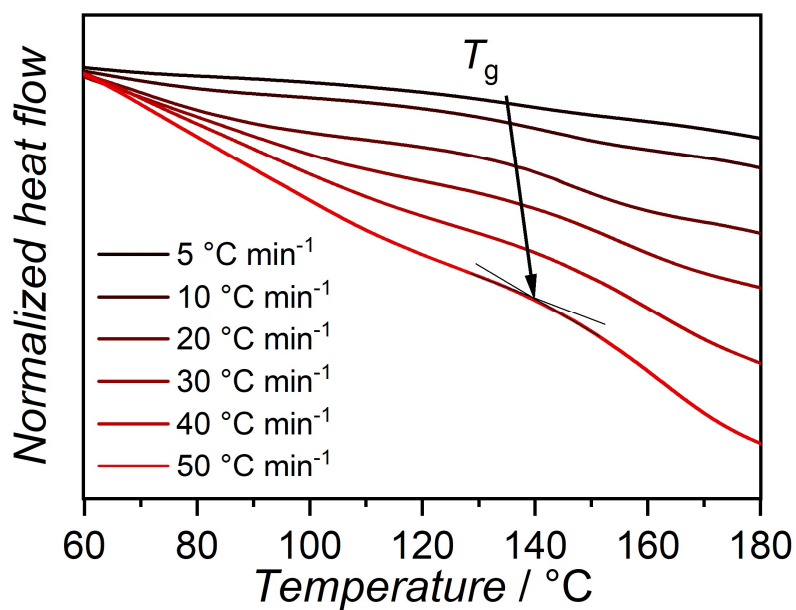


Fig. S13. DSC profile from 60 to 180 °C of **2g(Co)** with Ar flow. Heating rates were in the range of 5 to 50 °C min⁻¹.

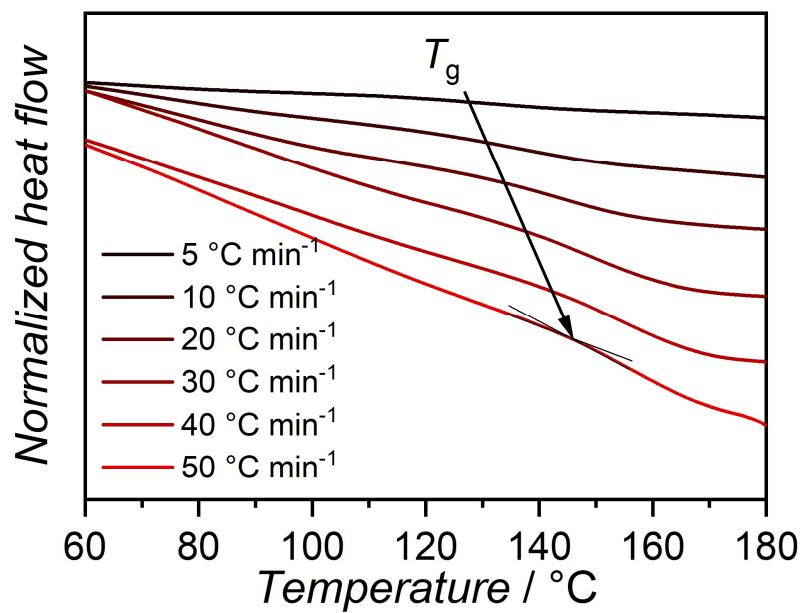


Fig. S14. DSC profile from 60 to 180 °C of **3g(Co)** with Ar flow. Heating rates were in the range of 5 to 50 °C min⁻¹.

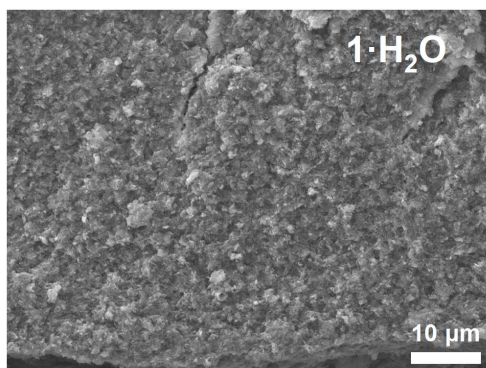


Fig. S15. Cross-section SEM image of **1·H₂O** crystalline pellet.

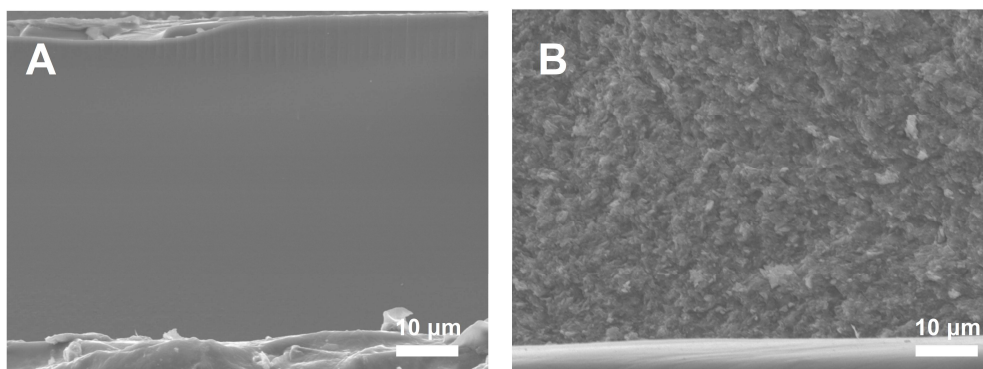


Fig. S16. (A) Cross-section SEM image of **2g(Co)** monolith. (B) Cross-section SEM image of **2·H₂O** crystalline pellet.

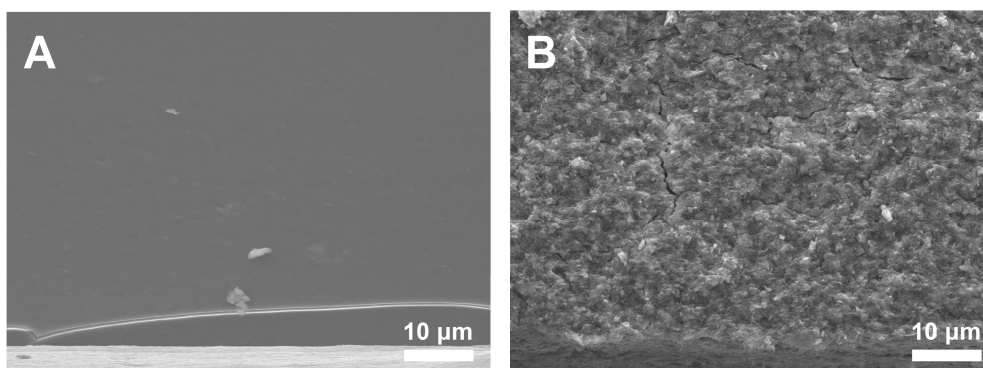


Fig. S17. (A) Cross-section SEM image of **3g(Co)** monolith. (B) Cross-section SEM image of **3·H₂O** crystalline pellet.

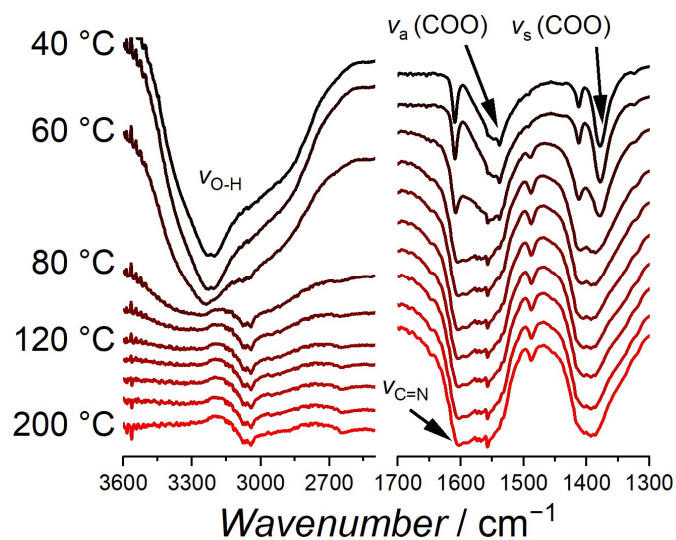


Fig. S18. VT-IR spectra of **1·H₂O** from room temperature to 200 °C with interval of 20 °C. The measurement was carried out in N₂ flow.

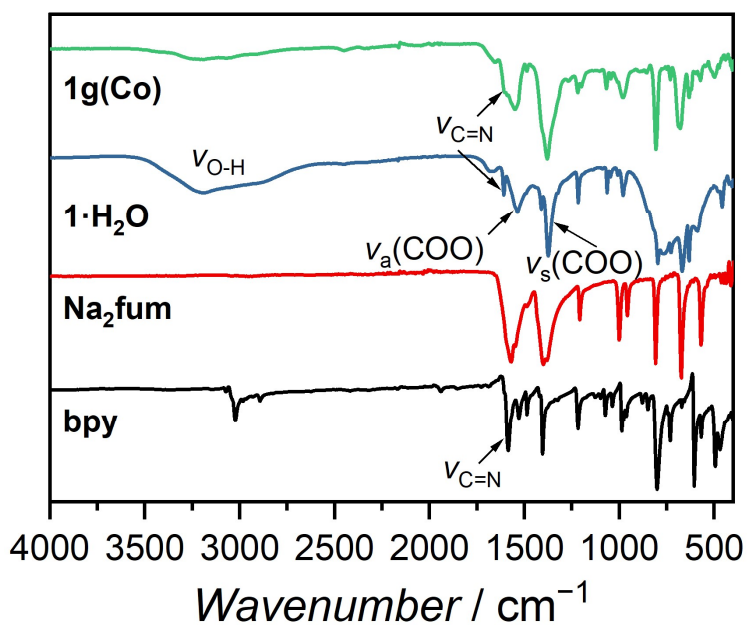


Fig. S19. FT-IR spectra of **1·H₂O**, **1g(Co)**, **Na₂fum** and **bpy** under Ar atmosphere at 25 °C.

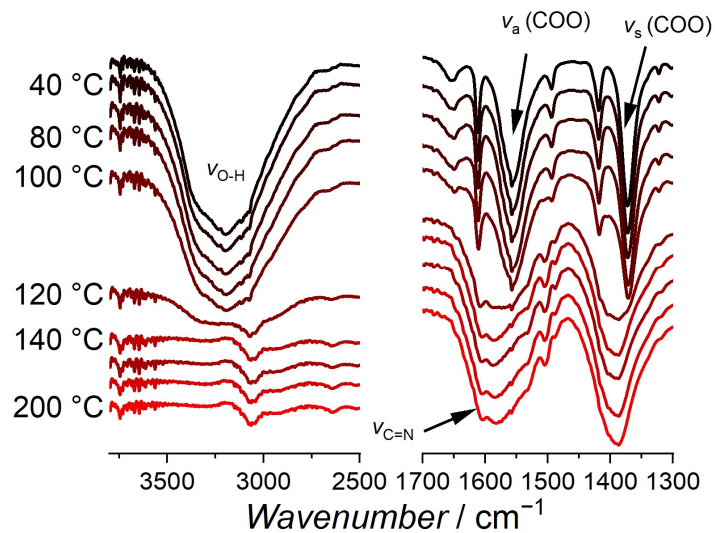


Fig. S20 VT-IR spectra of $2\cdot\text{H}_2\text{O}$ from room temperature to 200 °C with interval of 20 °C. The measurement was carried out in N_2 flow.

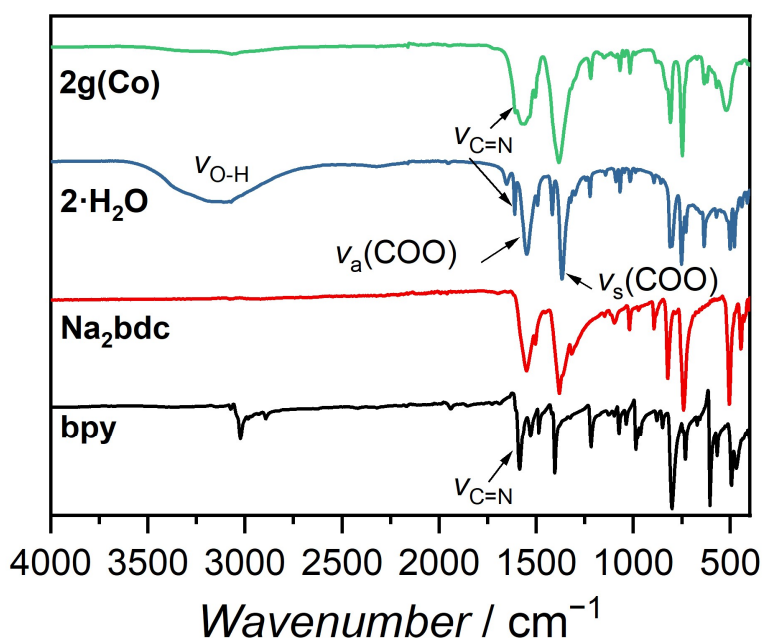


Fig. S21. FT-IR spectra of $2\cdot\text{H}_2\text{O}$, $2\text{g}(\text{Co})$, Na_2bdc and bpy under Ar atmosphere at 25 °C.

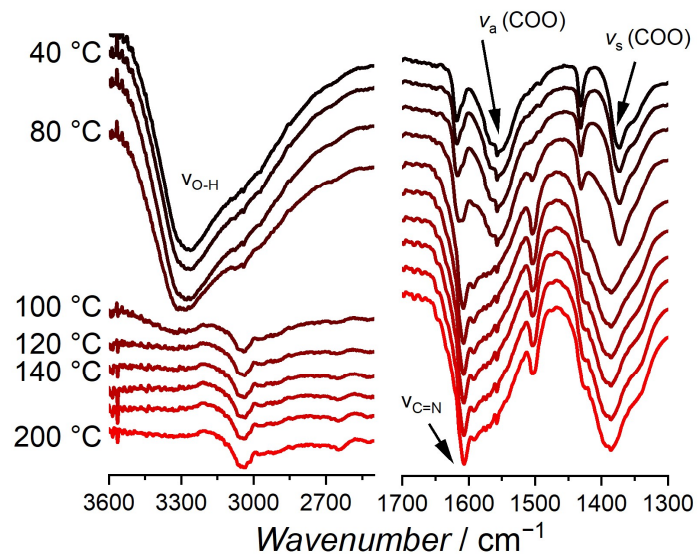


Fig. S22. VT-IR spectra of $3 \cdot \text{H}_2\text{O}$ from room temperature to 200 °C with interval of 20 °C. The measurement was carried out in N_2 flow.

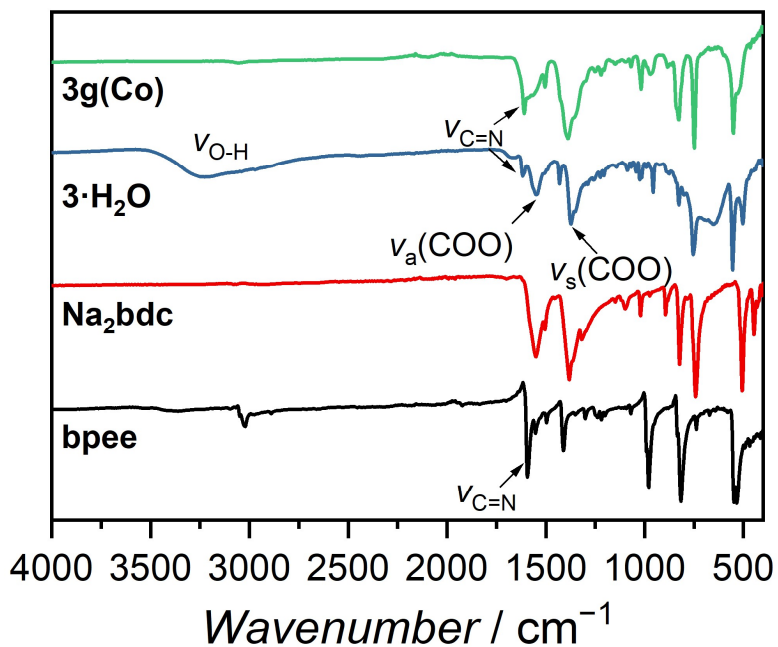


Fig. S23. FT-IR spectra of $3 \cdot \text{H}_2\text{O}$, $3\text{g}(\text{Co})$, Na_2bdc and bpee under Ar atmosphere at 25 °C.

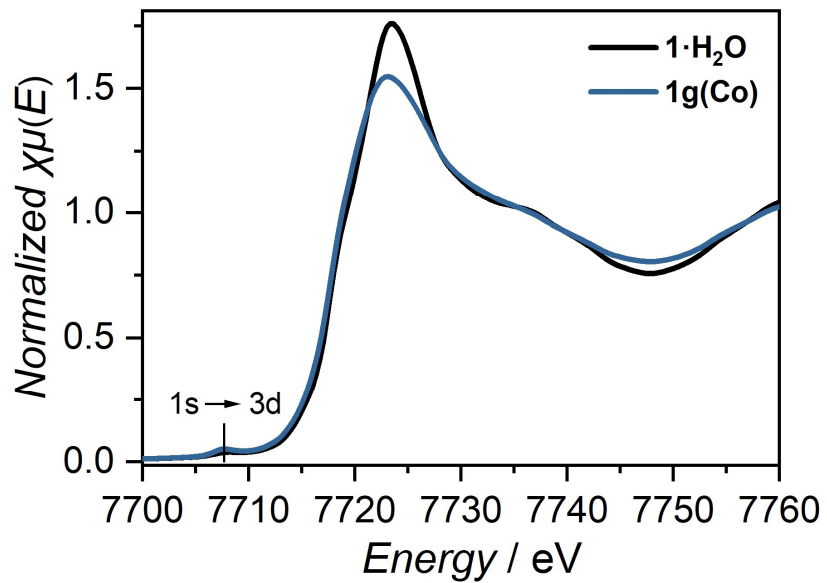


Fig. S24. XANES spectra of **1·H₂O** and **1g(Co)** under Ar at 25 °C.

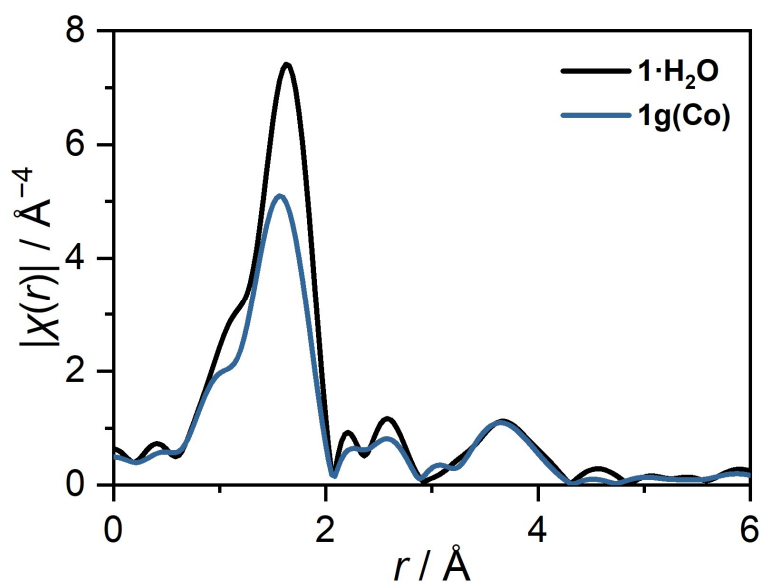


Fig. S25. EXAFS of **1·H₂O** and **1g(Co)** under Ar at 25 °C.

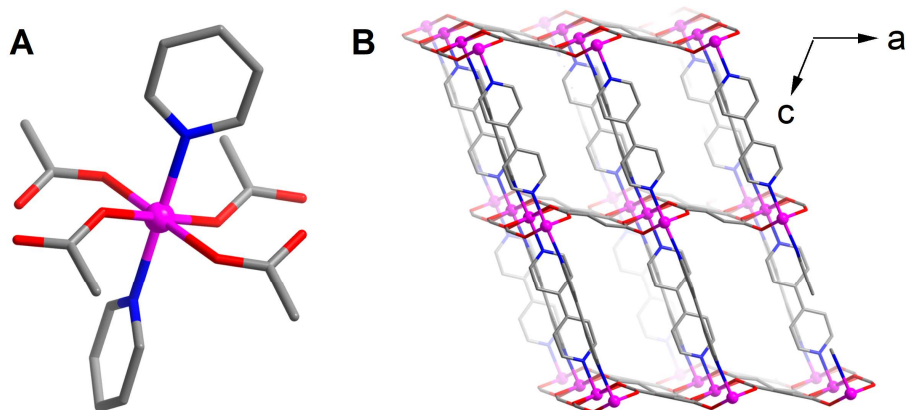


Fig. S26. Crystal structure of [Co(bpy)(fum)]. Gray, blue, red and violet are C, N, O and Co atoms, respectively. Guest molecules and H atoms on bpy and fum ligands are omitted for clarity.

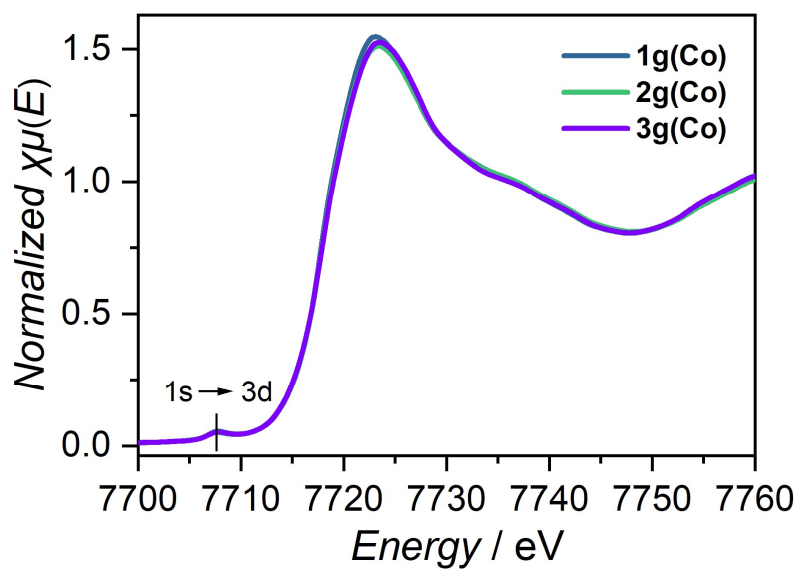


Fig. S27. XANES spectra of **1g(Co)**, **2g(Co)** and **3g(Co)** under Ar at 25 °C.

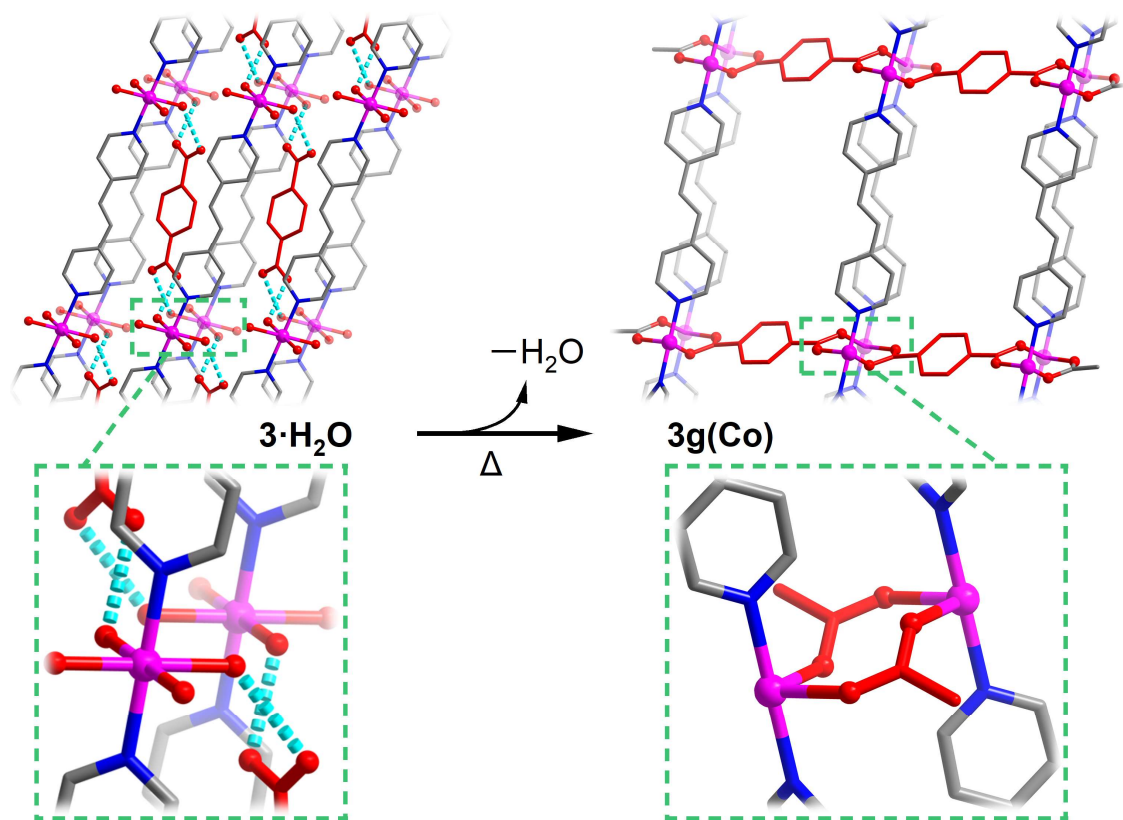


Fig. S28. Proposed structural transformation of $3 \cdot H_2O$ upon thermal dehydration. Hydrogen bonds between 1D $[Co(bpee)(H_2O)_4]^{2+}$ chain and bdc (2.69 and 2.77 Å) are shown as sky-blue dotted lines. Gray, blue, red and violet are C, N, O and Co atoms, respectively. Dicarboxylate ligands are in red colour. Solvent water molecules and hydrogen atoms are omitted for clarity.

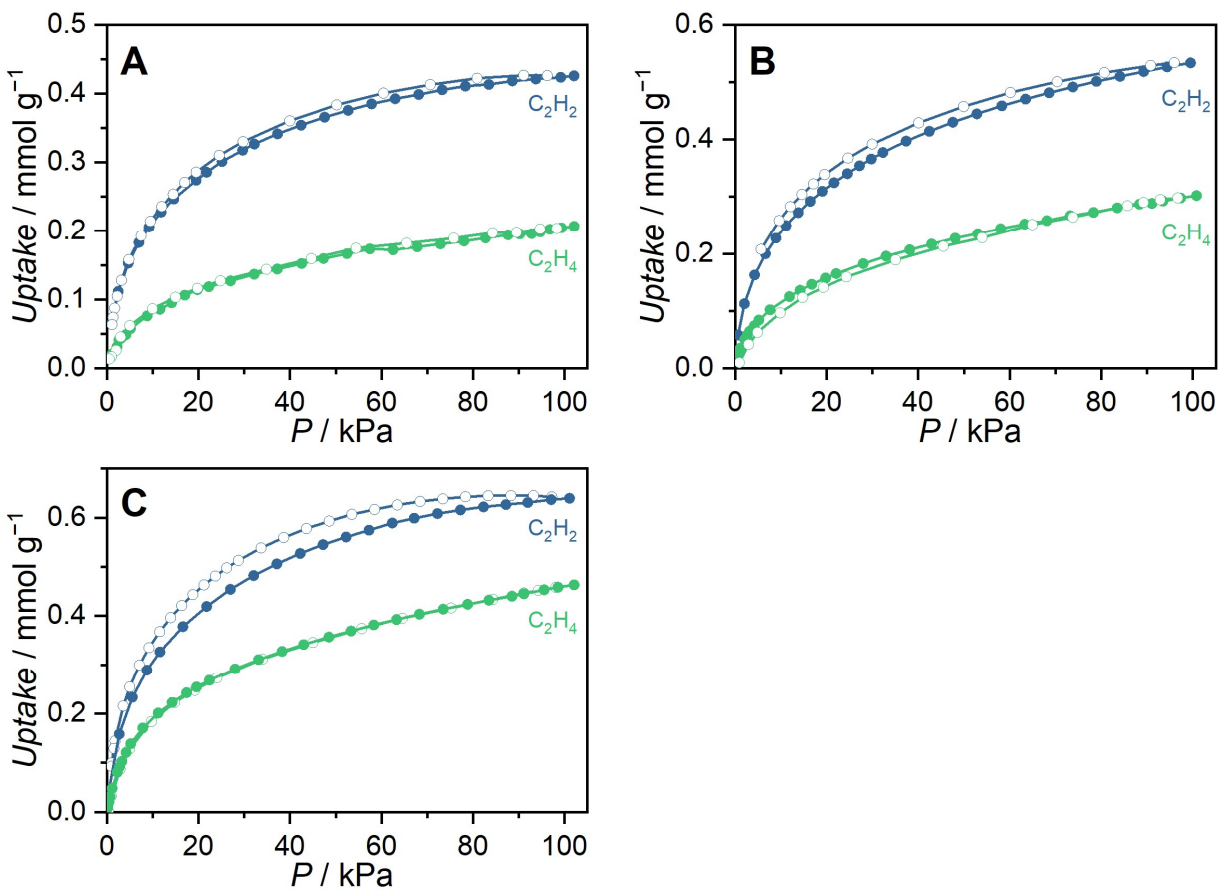


Fig. S29. Acetylene (C_2H_2) and ethylene (C_2H_4) adsorption isotherms of (A) **1g(Co)**, (B) **2g(Co)** and (C) **3g(Co)** at 273 K.

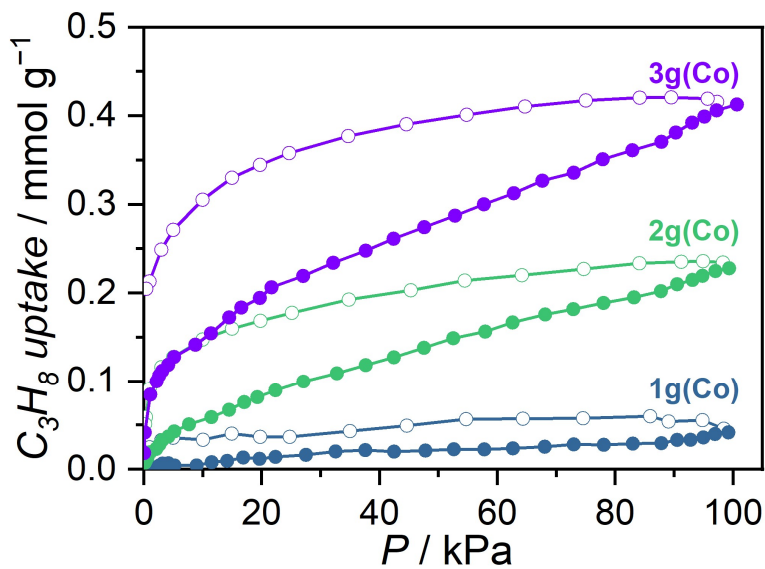


Fig. S30. n -Propane ($n-C_3H_8$) adsorption isotherms of **1g(Co)**, **2g(Co)** and **3g(Co)** at 273 K.

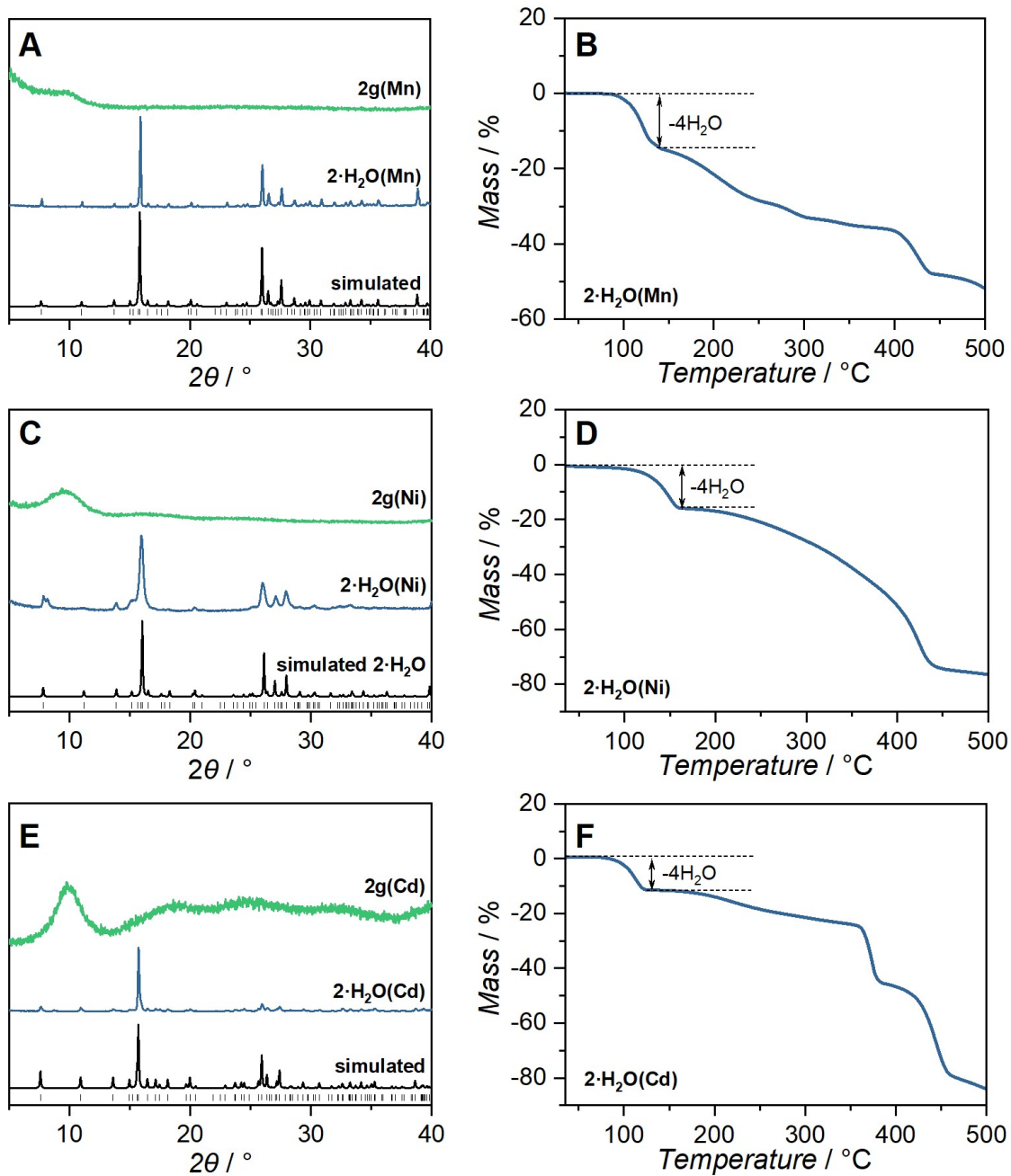


Fig. S31. PXRD and TGA profiles of (A, B) $2\cdot\text{H}_2\text{O}(\text{Mn})$, (C, D) $2\cdot\text{H}_2\text{O}(\text{Ni})$ and (E, F) $2\cdot\text{H}_2\text{O}(\text{Cd})$. Heating rates were $10\text{ }^\circ\text{C min}^{-1}$.

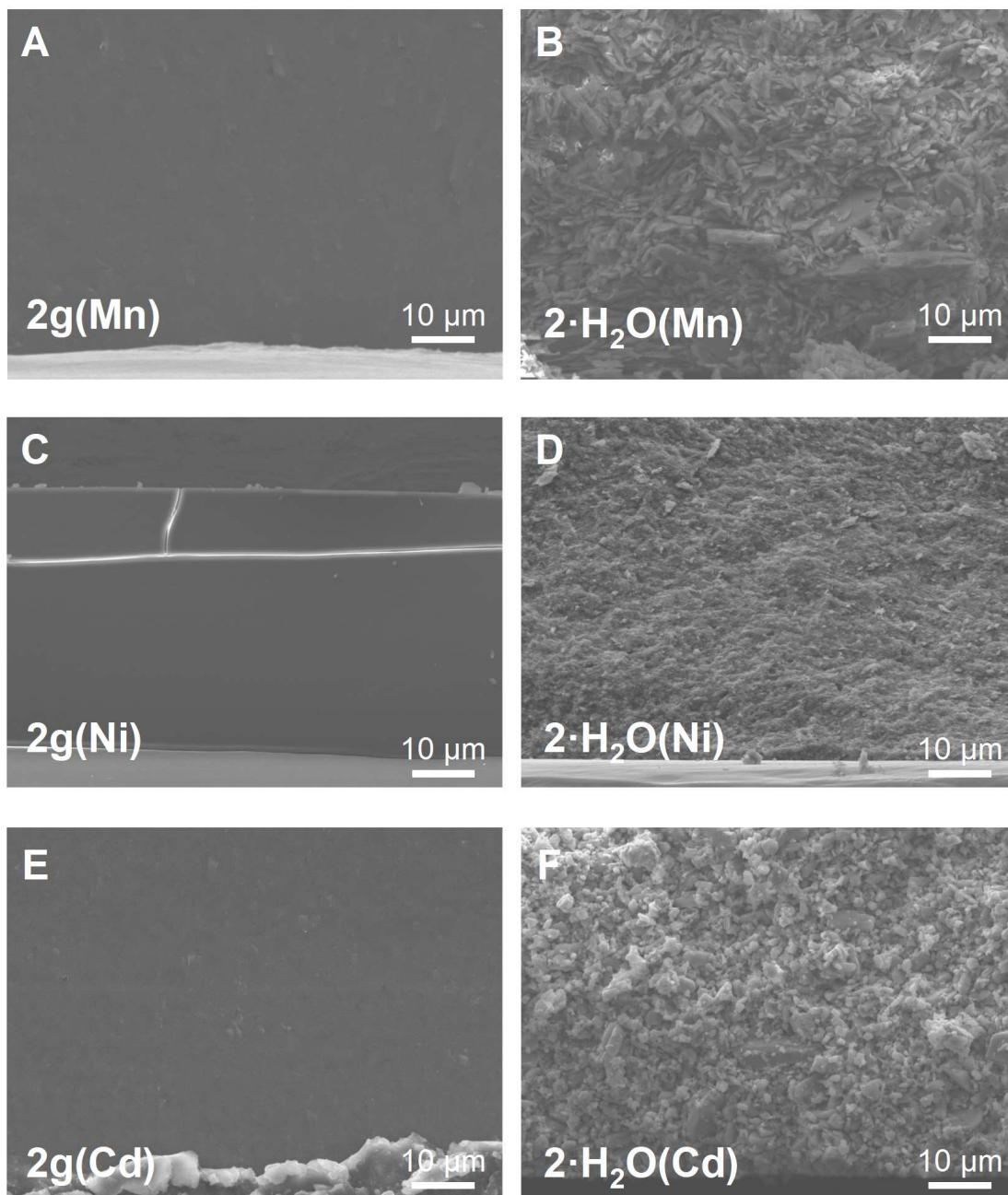


Fig. S32. Cross-section SEM images of (A) **2g(Mn)**, (B) **2·H₂O(Mn)**, (C) **2g(Ni)**, (D) **2·H₂O(Ni)**, (E) **2g(Cd)**, (F) **2·H₂O(Cd)**.

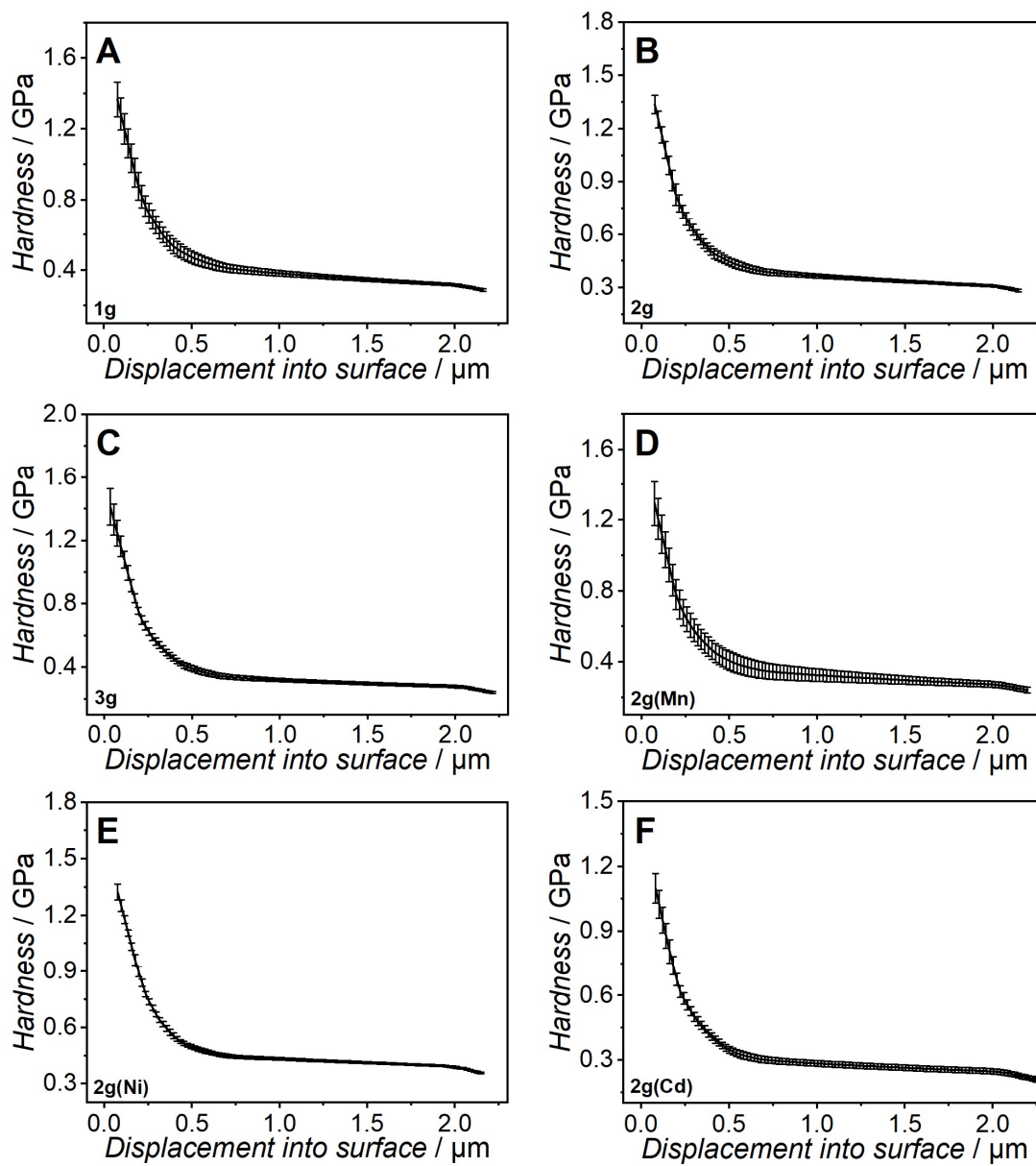


Fig. S33. Variation of hardness as a function of the indenter displacement in glass monoliths with standard deviation calculated based on 20 cycles of repeated tests.

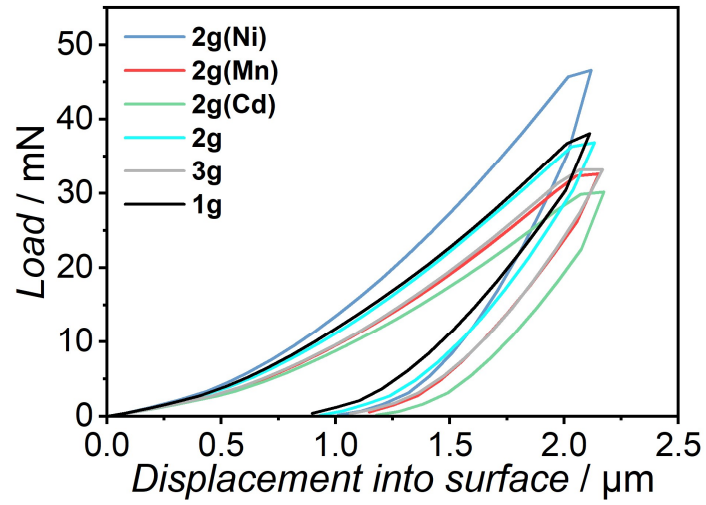


Fig. S34. Representative indentation load–displacement curves of glass monoliths.

Supplementary Tables:

Table S1. Elemental analysis of **1·H₂O**, **2·H₂O**, **3·H₂O**, **1g(Co)**, **2g(Co)** and **3g(Co)**.

Sample	Calculated			Experimental		
	C/%	H/%	N/%	C/%	H/%	N/%
1·H₂O	35.49	5.49	5.91	34.33	5.53	5.68
2·H₂O	47.91	4.47	6.21	47.81	4.41	5.98
3·H₂O	46.75	5.06	5.45	46.63	5.17	5.26
1g(Co)	51.06	3.04	8.51	50.15	3.39	7.82
2g(Co)	56.99	3.16	7.39	55.92	3.35	7.16
3g(Co)	59.21	3.45	6.90	58.48	3.72	6.71

Table S2. EXAFS fitting parameters of **1g(Co)**. $R^2=0.027$

Path	<i>Path degeneracy</i>	S_0^2	$\Delta E_0 / \text{eV}$	$R / \text{\AA}$	σ^2
Co-O	4.0±0.2	1.0	2.3±0.6	2.04±0.01	0.006
Co-N	2.0±0.2	1.0	2.3±0.6	2.20±0.01	0.003
Co-C	4.1±0.6	1.0	2.3±0.6	2.80±0.04	0.003
Co-C	4.0±0.4	1.0	2.3±0.6	2.99±0.04	0.004
Co-O	1.9±0.5	1.0	2.3±0.6	3.29±0.06	0.003

Table S3. Total gas uptake amount V_{ads} (mmol g⁻¹) of CO₂ at 195 K and the corresponding micropore volumes V_{pore} (cm³ g⁻¹) of glasses in this study.

Material	V_{ads} (mmol g ⁻¹)	V_{pore} (cm ³ g ⁻¹)
1g(Co)	0.94	0.03
2g(Co)	1.51	0.05
3g(Co)	2.08	0.07

Table S4. Total gas uptake amount (mmol g⁻¹) of hydrocarbons at 273 K of glasses in this study.

Gas / kinetic diameter (Å)	1g(Co)	2g(Co)	3g(Co)
C ₂ H ₂ / 3.3	0.43	0.53	0.64
C ₂ H ₄ / 4.2	0.21	0.30	0.46
<i>n</i> -C ₃ H ₈ / 4.3	0.04	0.23	0.41

Table 5. Mechanical properties of glass monoliths based on indentation measurements in this study.

Glass monolith	<i>Hardness H / GPa</i>	<i>Young's modulus E / GPa</i>
1g(Co)	0.28	4.49
2g(Co)	0.27	4.70
3g(Co)	0.24	4.51
2g(Mn)	0.24	4.16
2g(Ni)	0.35	4.94
2g(Cd)	0.22	4.33

References:

1. S. C. Manna, S. Konar, E. Zangrando, K. i. Okamoto, J. Ribas and N. Ray Chaudhuri, *Eur. J. Inorg. Chem.*, 2005, 4646-4654.
2. Y.-R. Pan, L.-B. Wang, P.-Y. Zhan, Y.-L. Niu and G.-Q. Zhang, *Acta crystallogr. E*, 2006, **62**, m3034-m3035.
3. L. Frenzel-Beyme, P. Kolodzeiski, J. B. Weiss, A. Schneemann and S. Henke, *Nat. Commun.*, 2022, **13**, 7750.
4. T. E. Faber and J. M. Ziman, *Philos. Mag.*, 1965, **11**, 153-173.
5. E. Lorch, *J Phys Part C Solid*, 1969, **2**, 229.
6. S. Kohara, M. Itou, K. Suzuya, Y. Inamura, Y. Sakurai, Y. Ohishi and M. Takata, *J. Physics: Condens. Matter.*, 2007, **19**, 506101.